JACS
JOURNAL OF THE AMERICAN CHEMICAL SOCIETY
Article
pubs.acs.org/JACS

NH^{2-} Dianion Entrapped in a Nanoporous $12CaO{\cdot}7Al_2O_3$ Crystal by Ammonothermal Treatment: Reaction Pathways, Dynamics, and Chemical Stability

Fumitaka Hayashi,*[,†,⊥] Yudai Tomota,[‡] Masaaki Kitano,[§] Yoshitake Toda,[†,∥] Toshiharu Yokoyama,[∥] and Hideo Hosono*[,†,‡,§,∥]

[†]Frontier Research Center, Tokyo Institute of Technology, 4259-S2-13 Nagatsuta, Midori-ku, Yokohama 226-8503, Japan
[‡]Materials and Structures Laboratory, Tokyo Institute of Technology, 4259 Nagatsuta, Midori-ku, Yokohama 226-8503, Japan
[§]Materials Research Center for Element Strategy, Tokyo Institute of Technology, 4259 Nagatsuta, Midori-ku, Yokohama 226-8503, Japan
[∥]Accel Program, Japan Science and Technology Agency (JST), 4-1-8 Honcho, Kawaguchi, Saitama 332-0012, Japan

Supporting Information

ABSTRACT: Inorganic imides are useful for hydrogen storage and base-catalyzed reactions but are extremely unstable under ambient conditions, which hinders their practical use as functional materials. Here, we demonstrate that NH_2^- and H^-, as well as NH^{2-}, can be incorporated into the nanocages of the mayenite crystals, $[Ca_{24}Al_{28}O_{64}]^{4+}(e^-)_4$ and $[Ca_{24}Al_{28}O_{64}]^{4+}(O^{2-})_2$, by ammonothermal treatment. We evaluated the reaction conditions and found that the anion exchange reaction proceeded at higher than 500 °C. Raman spectroscopy showed that the N−H band position of encaged NH^{2-} was close to that of CaNH and MgNH crystals. We also studied the reaction pathways that yield NH_2^- and NH^{2-} anions and their dynamic motions by ^1H NMR spectroscopy. Successive reactions of encaged e^- and O^{2-} ions with NH_3 yielded NH_2^-, NH^{2-}, and H^- or OH^-, in which the O^{2-} ion reacted more efficiently with NH_3. The maximum NH^{2-} concentration and content were ~2.7×10^{20} cm^{-3} and ~0.25 (wt %)$_{NH}$, respectively. The short spin−lattice relaxation time found in ^1H NMR suggests that the incorporated NH_2^- and NH^{2-} rotate or librate in the cage near room temperature. Stability tests showed that the encaged NH^{2-} ions are chemically stable under ambient conditions and in organic solvents. These results are attributed to the encapsulation of active anions within subnanometer-sized cages composed of Ca−O−Al oxide frameworks. The encaged NH^{2-} desorbed as NH_3 at higher than 500 °C under vacuum (E_a = 172 kJ mol^{-1}). It is thus expected that $C_{12}A_7{:}NH^{2-}$ will function as a reactive nitrogen source for nitrogen transfer reactions by in situ cage degradation.

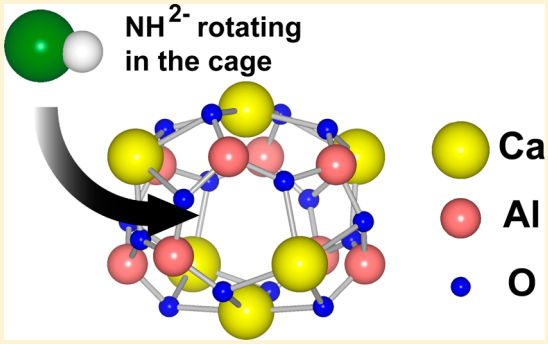

INTRODUCTION

Inorganic imide compounds bearing an NH^{2-} group, such as Li_2NH, MgNH, and EuNH, have attracted attention because of potential applications requiring their high hydrogen storage capacity[1,2] and strong solid basicity.[3] Among inorganic imides, NH^{2-} anions with size of 0.27 nm in diameter can be stabilized as ionic compounds by Coulomb interactions with metal cations. However, NH^{2-}-bearing compounds are extremely unstable under ambient conditions or in polar organic solvents such as alcohols because of their strong Brönsted basicity, leading to difficulties in various applications. Therefore, chemically stable inorganic imides are needed for these applications. Encapsulation within the inner space of nanoporous materials or molecular containers such as zeolites and metal−organic frameworks (MOFs) is an effective method to modulate the reactivity of molecules and ions. For instance, a monomeric aldehyde susceptible to polymerization can be stored under ambient conditions in the supercage (diameter ~0.8 nm) of a NaY zeolite, wherein it is activated enough to react with nucleophiles.[4] As another successful example, an air-sensitive P_4 molecule is rendered chemically stable within a hydrophobic cavity (diameter, ~0.2 nm) of a self-assembled Fe-based MOF.[5] Various anion receptors have been successfully developed using supermolecular chemistry concepts,[6] but the encapsulation of highly reactive anions like NH^{2-} within the cavities of metallomacrocycles and metallocages has not been successful to date.

A nanoporous crystal $12CaO{\cdot}7Al_2O_3$, abbreviated as $C_{12}A_7{:}O^{2-}$, is a fast oxygen ion conductor that possesses extraframework oxygen ions in subnanometer-sized cages.[7] It is convenient to describe its unit cell, which is composed of two

Received: April 27, 2014
Published: July 30, 2014

   dx.doi.org/10.1021/ja504185m | J. Am. Chem. Soc. 2014, 136, 11698−11706

formula units ($Z = 2$) as $[Ca_{24}Al_{28}O_{64}]^{4+}\cdot 2O^{2-}$. In contrast to aluminosilicate zeolites, $C_{12}A_7{:}O^{2-}$ has a positively charged lattice framework $[Ca_{24}Al_{28}O_{64}]^{4+}$, in which the positive charge of the cage wall is compensated by anions that are accommodated within subnanocages of ∼0.44 nm in diameter. Its O^{2-} ions can be replaced with various anions such as H^-,[8a] F^-,[8b] Au^-,[8c] and electrons,[9] by chemical/physical treatments. Table S1, Supporting Information, summarizes the sizes of the accommodated anions. Electron-embedded $C_{12}A_7$, denoted $C_{12}A_7{:}e^-$, is an electride in which electrons act as anions.[10] Recently, German and Norwegian research groups independently reported that an NH_2^- monoanion could be incorporated into the cage of $C_{12}A_7{:}O^{2-}$ through nitridation with gaseous NH_3 at 950 °C for 10 h.[11] The nitrogen content and concentration were ∼1.0 (wt %)$_N$ and ∼1.1 × 10^{21} cm^{-3}, respectively.

Liquid/supercritical NH_3 is a good solvent for the dissolution of alkali, alkaline earth, and certain rare earth metals, resulting in the formation of solvated electrons.[12,13] We thus tried dissolving $C_{12}A_7{:}e^-$ in supercritical NH_3, but the dissolution reactions did not proceed, even at high temperatures. Instead, during this experiment, we found that the NH_3 molecules react with encaged electrons in the $C_{12}A_7{:}e^-$ or encaged O^{2-} ions in $C_{12}A_7{:}O^{2-}$ upon ammonothermal treatment at 500 °C or higher, leading to the successive introduction of NH_2^-, NH^{2-}, H^-, and OH^- to the cages. As far as we know, this is the first demonstration of an encapsulated NH^{2-} dianion within a nanometer-sized space. The reaction pathways, dynamics, and chemical stability of the NH_2^- and NH^{2-} species were studied using ^{1}H nuclear magnetic resonance (NMR) and temperature-programmed desorption (TPD) spectroscopies in addition to immersion tests in organic solvents. Finally, a potential application of $C_{12}A_7{:}NH^{2-}$ is discussed.

EXPERIMENTAL SECTION

Materials. Two kinds of $C_{12}A_7{:}e^-$ with different electron concentrations were prepared according to established procedures[14] using Ti metal as a reducing agent. $C_{12}A_7{:}e^-$ with an electron concentration of 1.1 × 10^{21} cm^{-3} was designated $C_{12}A_7{:}e^-_{half}$, while that with 2.3 × 10^{21} cm^{-3} was designated $C_{12}A_7{:}e^-_{full}$ based on the fact that the theoretical maximum of encaged electrons is 2.3 × 10^{21} cm^{-3}, which corresponds to the positive charge of the cage wall. $C_{12}A_7{:}O^{2-}$, which was obtained from $CaCO_3$ and γ-Al_2O_3 by calcination at 1300 °C for 6 h, CaO (15 m^2 g^{-1}, Kojundo), α-Al_2O_3 (10 m^2 g^{-1}, Kojundo), and $CaO{\cdot}Al_2O_3$ (abbreviated CA and synthesized from $CaCO_3$ and γ-Al_2O_3) were used for comparison. As a reference sample, $Ca(NH_2)_2$ was prepared by the immersion of Ca metal in liquid NH_3 at 150 °C and 15 MPa, while CaNH was prepared by the heat treatment of Ca_3N_2 at 500 °C in a flow of H_2 and N_2. Figure S1, Supporting Information, shows the XRD patterns of $Ca(NH_2)_2$ and CaNH crystals. The latter accounted for 91.7% of the CaNH and 8.3% of the CaH_2 from a Rietvelt analysis. The crystal structures of $Ca(NH_2)_2$ and CaNH are shown in Figure S2, Supporting Information.[15,16] In the former, the amide ions are subjected to a fast librational motion.[15] In the latter, the H atoms bound to the N atoms are disordered. The Ca and N atoms are here arranged so that they form a NaCl-type structure (Figure S2b, Supporting Information).

Ammonothermal Treatment. Ammonothermal treatment was carried out at 35−55 MPa and at 400−600 °C using a cone closure vessel (6.3 mm i.d., Parker Autoclave Engineers, Inc., USA). Typically, a 200 mg sample (as ground powder) and 5−7 g of $^{14}NH_3$ (99.9999%, Air Liquide Japan Co. Ltd., Japan) were mounted on the reactor, and then the temperature was increased to 400−600 °C and was maintained for 3 h. When required, $^{15}NH_3$ (98% as $^{15}NH_3$, SI Science Co. Ltd., Japan) was used as a nitrogen source instead of $^{14}NH_3$.

Characterization. Raman spectra were collected using an HR-800 spectrometer (Horiba Jobin Yvon, Japan). CW-DPSS laser light (λ = 457.4 nm, 50 mW) was focused onto the sample surface through an objective lens, and an energy cutoff filter was used to prevent thermal decomposition induced by laser irradiation. DC magnetization was measured using a vibrating sample magnetometer (SVSM, Quantum Design, USA) under a high magnetic field of 10000 Oe. XRD patterns were recorded using a D8 Advance diffractometer (Bruker) with monochromated Cu Kα radiation (λ = 0.15418 nm, 45 kV, 360 mA). The lattice constants were determined by a Rietvelt analysis. Raman spectra and XRD patterns of $Ca(NH_2)_2$ and CaNH were measured under an argon atmosphere in airtight holders.

Solid-state ^{1}H magic angle spinning (MAS) NMR and ^{15}N cross-polarization (CP) and dipolar decoupling (DD) MAS NMR spectra were recorded using a JEOL JNM-ECA 500II 495.1 MHz spectrometer at a 10 kHz spin rate, wherein the sample was loaded into a 4 mm pencil-type zirconia rotor under ambient conditions or under an argon atmosphere. The recycle delays and scan times for ^{1}H MAS, ^{15}N CP-MAS, and ^{15}N DD-MAS NMR measurements were 100−185, 50, and 60 s and 8−16, 1024, 4096 times, respectively. The external chemical shift references were silicone rubber (−0.12 ppm for ^{1}H MAS NMR) and $^{15}NH_4Cl$ (−341.17 ppm for ^{15}N CP- and DD-MAS NMR). The spin−lattice relaxation time T_1 for ^{1}H spin was measured using the pulse sequence 180°−τ−90° in the inversion recovery method wherein τ is the duration time. The T_1 values were estimated from the correlation $\ln(M_0 - M(\tau)) = -\tau/T_1 + \ln(2M_0)$ wherein M_0 is the signal intensity at τ = 60−150 s.

The electron concentrations in the mayenite samples were determined by iodometry.[17] The total amount of NH_2^-/NH^{2-} ions was determined by ion chromatography (IC)[18] or TPD analysis.[19] In the former, typically 5−30 mg of sample was dissolved in HCl or HF aqueous solutions (0.5−2.0 cm^3). The amount of resulting NH_4^+ was quantitatively analyzed by IC with a CDD-10A conductivity detector (Shimadzu, Japan). An IC-C4 column (Shimadzu) was used for the separation, and the eluant was a 2.0 mM oxalic acid aqueous solution. In the latter, the amount of $^{14}NH_3$ evolved from the sample was determined from the integration of peak area, m/z = 16, using a TDS1200 (ESCO, Japan) instrument operating at ∼10^{-6} Pa. Typically, 0.5−5 mg of sample was used for the measurement. The detection limit for the N content of the sample was ∼0.0001 (wt %)$_N$, which corresponds to a nitrogen concentration of ∼0.01 × 10^{19} cm^{-3}. The NH^{2-}, NH_2^-, H^-, and OH^- concentrations were estimated from their respective peak areas in the ^{1}H NMR spectra and the total amounts of NH_2^-/NH^{2-}.

Stability Tests. The chemical stability of $C_{12}A_7{:}NH^{2-}$ was studied under ambient conditions and in polar organic solvents such as methanol (MeOH) and tetrahydrofuran (THF). In the former, ∼100 mg of sample was stored for 40 days in air at room temperature, while in the latter ∼50 mg of sample was immersed in the solvent for 10 min at room temperature.

RESULTS AND DISCUSSION

Reactivity of Encaged Electrons with Supercritical NH_3. We first examined the synthetic conditions for $C_{12}A_7{:}NH^{2-}$ using $C_{12}A_7{:}e^-_{half}$ as a starting material. Figure 1a shows Raman spectra of $^{14}NH_3$-treated $C_{12}A_7{:}e^-_{half}$ as a function of reaction temperature. The NH_3 treatment at 400 °C did not change the spectrum of the parent $C_{12}A_7{:}e^-_{half}$, but the treatment at 500 °C yielded broad bands at 3200−3300 cm^{-1} and a sharp band at 3560 cm^{-1}. The latter is assigned to the stretching mode of OH^- entrapped in a nanocage, which is readily formed through wet air treatment at 800−1000 °C.[20] After treatment at 600 °C, the sharp peak at 3210 cm^{-1} is enhanced while the broad peak around 3270 cm^{-1} and sharp peak at 3560 cm^{-1} are reduced. Additionally, no peak is present between 1000 and 2000 cm^{-1} in which peaks arising from the bending mode of the nitrogen and oxygen species associated with hydrogen like NH_2^- should appear. Figure 1b shows

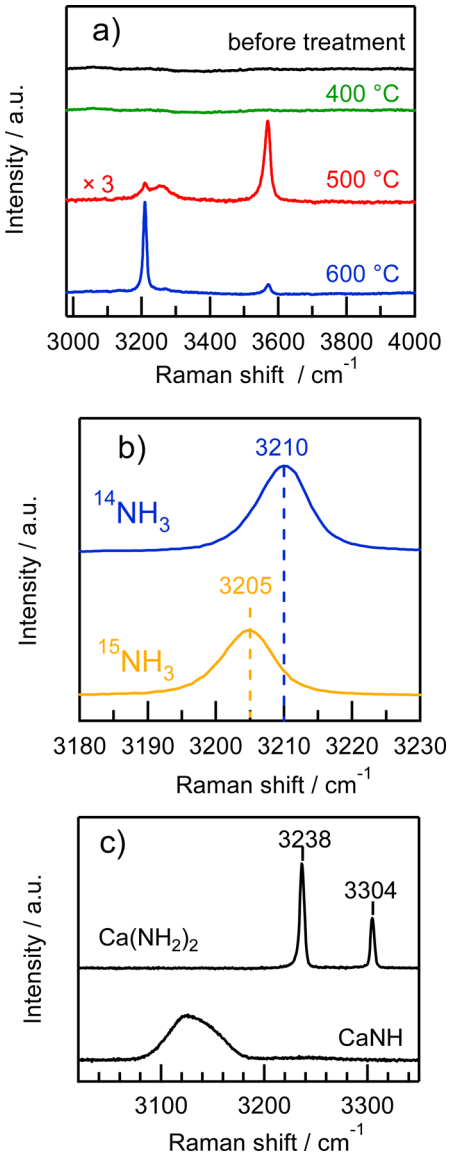

Figure 1. (a) Raman spectra of parent $C_{12}A_7{:}e^-_{half}$ (black line) and $^{14}NH_3$-treated $C_{12}A_7{:}e^-_{half}$ at 400 (green line), 500 (red line), and 600 °C (blue line). (b) Isotope effect on the band position of encaged NH^{2-}: $^{14}NH_3$ (blue line) and $^{15}NH_3$ (yellow line) treated $C_{12}A_7{:}e^-$ at 600 °C. (c) Raman spectra of $Ca(NH_2)_2$ and CaNH crystals.

Raman spectra of $^{15}NH_3$-treated $C_{12}A_7{:}e^-_{half}$ at 600 °C. The band at 3210 cm^{-1} was red-shifted by 5 cm^{-1} compared with that for the $^{14}NH_3$-treated $C_{12}A_7{:}e^-_{half}$. The extent of this shift is in good agreement with that expected from the simple isotope effect ($3210 \times (14/15)^{1/2}/(15/16)^{1/2} = 3203$). Therefore, the sharp peak at 3210 cm^{-1} is attributed to the stretching mode of NH^{2-}. Figure 1c shows Raman spectra of the $Ca(NH_2)_2$ and CaNH crystals. $Ca(NH_2)_2$ gave two sharp bands that peak at 3238 and 3304 cm^{-1}, and these are in good agreement with those of $Ca(NH_2)_2$ (3235, 3304 cm^{-1}) in the literature.[21] On the other hand, CaNH gave a broad band centered at 3140 cm^{-1}, which results from the disordered H atom positions in the crystal (see Figure S2b, Supporting Information). This band position agrees well with that (3130 cm^{-1}) reported by Kojima and Kawai[22] and is somewhat shifted in the lower region compared with the previous results of CaNH (~3180 cm^{-1}).[23] It is worth noting that the present study and the report by Kojima and Kawai show the XRD patterns of CaNH crystals, which is informative to the interpretation of Raman/IR data. In contrast, the latter two studies[23] show no XRD results. Since the broad band at 3270 cm^{-1} from the $C_{12}A_7{:}NH^{2-}$ prepared at 500 °C is rather close to the band for $Ca(NH_2)_2$, we tentatively assigned this band to the stretching mode of NH_2^-, which may be regarded as an intermediate species for NH^{2-}.

Here, we compared the band position of the NH^{2-} encapsulated in the nanocage with that observed for other crystalline inorganic imides. Figure 2 shows the reported

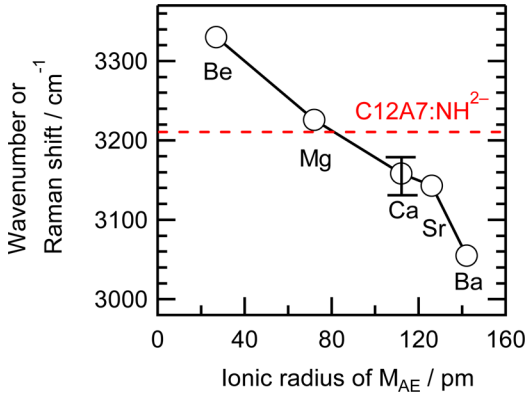

Figure 2. Correlation between the ionic radius of alkaline earth metals (M_{AE} = Be, Mg, Ca, Sr, or Ba) and the peak position of NH^{2-} in $M_{AE}NH$ according to the data in refs 22 and 23. Dashed red line shows the peak position for $^{14}NH_3$-treated $C_{12}A_7{:}e^-_{half}$ at 600 °C.

correlation between the band position of NH^{2-} in $M_{AE}NH$ (M_{AE} = Be, Mg, Ca, Sr, or Ba) and the ionic radius of M_{AE}.[22,23] The peak position of the encaged NH^{2-} in the $C_{12}A_7$ crystal is between those of CaNH (3158 ± 25 cm^{-1})[22,23] and MgNH (3226 cm^{-1}).[22] This observation appears to be consistent because the Ca ions that constitute the cage wall coordinate to the caged NH^{2-} ion.

Magnetic measurements were carried out to examine whether the encaged NH^{2-} is paramagnetic. Figure S3a, Supporting Information, shows $M-T$ curves for the parent and the NH_3-treated $C_{12}A_7{:}e^-_{half}$ samples. The spin concentration was estimated using the Curie Law by assuming that $S = 1/2$ is ~5.0×10^{14} cm^{-3} for the parent $C_{12}A_7{:}e^-_{half}$ and ~1.0×10^{15} cm^{-3} for the NH_3-treated $C_{12}A_7{:}e^-_{half}$. Both these spin concentrations are about 5 orders of magnitude less than those of encapsulated NH_2^- or NH^{2-} determined by the IC, TPD, and ^1H NMR measurements, indicating that the encaged nitrogen species are not radicals like NH_2 and NH^-.

Figure S3b, Supporting Information, shows the XRD patterns of parent $C_{12}A_7{:}e^-_{half}$ and NH_3-treated $C_{12}A_7{:}e^-_{half}$ at 600 °C and 55 MPa. These two samples had diffraction peaks only assignable to mayenite (space group $I\bar{4}3d$, PDF 00-009-0413) and no peak(s) assignable to crystalline CaNH or $Ca(NH_2)_2$. Figure 3 shows the lattice constant a and the intensity ratio I_{420}/I_{211} of the 420 diffraction peak to the 211 diffraction peak for the NH_3-treated $C_{12}A_7{:}e^-_{half}$ samples as a function of reaction temperature. The I_{420}/I_{211} value is an index for the electron occupancy of anion sites in the $C_{12}A_7$ crystal.[9] The $C_{12}A_7{:}e^-$ samples have smaller I_{420}/I_{211} values because of the absence of anions with an atom core compared with $C_{12}A_7{:}O^{2-}$. The a value remained constant at 1.1995 nm at less than 400 °C and then decreased to 1.1978 nm upon

dx.doi.org/10.1021/ja504185m | J. Am. Chem. Soc. 2014, 136, 11698−11706

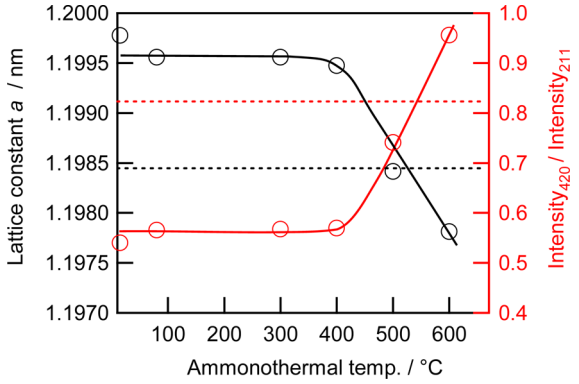

Figure 3. Lattice constant a and the intensity ratio I_{420}/I_{211} of the 420 diffraction peak to the 211 diffraction peak for the NH_3-treated $C_{12}A_7{:}e^-$ half samples as a function of reaction temperature. The dashed black and red lines show the results for the $C_{12}A_7{:}O^{2-}$.

ammonothermal treatment at 600 °C. The I_{420}/I_{211} value remained constant at less than 400 °C and then it increased. The decrease in a and the increase in the I_{420}/I_{211} value indicated the replacement of electrons by other extraframework anions like NH^{2-} and OH^-, which caused the displacement of two Ca framework ions that were axially coordinated to anions.[24]

The concentrations of various anions such as electrons, NH_2^-, NH^{2-}, H^-, and OH^- in the NH_3-treated $C_{12}A_7{:}e^-_{half}$ samples were determined by iodometry, IC, TPD, and NMR analyses and are summarized in Table 1 together with those for the parent $C_{12}A_7{:}e^-_{half}$. The electron concentration of the parent $C_{12}A_7{:}e^-_{half}$ was 1.1×10^{21} cm^{-3} (entry 1, Table 1). The electron and NH^{2-} concentrations remained unchanged upon ammonothermal treatment at 400 °C (entry 2 vs entry 1), indicating that $C_{12}A_7{:}e^-$ is chemically stable in supercritical NH_3 at lower than 400 °C. The concentrations of e^-, NH_2^-, and NH^{2-} after the 500 °C NH_3 treatment were 9.4×10^{20}, 0.01×10^{20}, and 0.24×10^{20} cm^{-3}, respectively (entry 3). It is possible to quantitatively distinguish NH^{2-} from NH_2^- in the ^1H MAS NMR spectra, as discussed in the next section. Measurable amounts ($(0.4–0.6) \times 10^{20}$ cm^{-3}) of H^- and OH^- were also detected (entry 3). The ammonothermal treatment at 600 °C further decreased the e^- concentration and increased the NH_2^-, NH^{2-}, H^-, and OH^- concentrations. The NH_2^- and NH^{2-} concentrations were 1.08×10^{20} and 1.45×10^{20} cm^{-3} (entry 4). The reaction pathways yielding NH_2^-, NH^{2-}, and H^- will be discussed in the next section.

Effect of Extraframework Anions on the Reaction Pathways. We investigated the effect of extraframework anions and cage structure on the incorporation of NH^{2-} using the $C_{12}A_7$ samples with different electron concentrations and non-nanoporous relevant materials. Figure 4 shows the

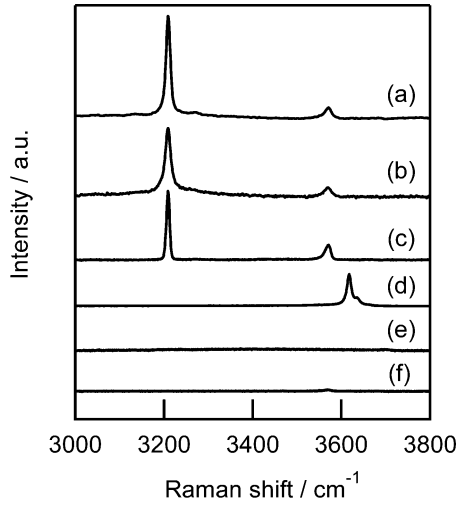

Figure 4. Raman spectra of $^{14}NH_3$-treated $C_{12}A_7{:}e^-_{half}$ (a), $C_{12}A_7{:}e^-_{full}$ (b), $C_{12}A_7{:}O^{2-}$ (c), CaO (d), α-Al_2O_3 (e), and $CaO{\cdot}Al_2O_3$ (f) at 600 °C and at 55 MPa. Samples a–c are the same as those in entries 4, 6, and 8 in Table 1

Raman spectra of the $^{14}NH_3$-treated $C_{12}A_7{:}e^-_{full}$, $C_{12}A_7{:}O^{2-}$, CaO, α-Al_2O_3, and $CaO{\cdot}Al_2O_3$ (CA) at 600 °C and 55 MPa together with that obtained from $C_{12}A_7{:}e^-_{half}$. The NH_3-treated $C_{12}A_7{:}e^-_{full}$ and $C_{12}A_7{:}O^{2-}$ gave a sharp signal at 3210 cm^{-1} as a result of the incorporation of the NH^{2-} dianion in the cage, in which the NH^{2-} concentrations were 0.52×10^{20} and 2.71×10^{20} cm^{-3}, respectively (entries 6 and 8 in Table 1). In contrast, the NH_3-treated CaO, α-Al_2O_3, and CA did not have peaks between 3200 and 3300 cm^{-1} indicating that the NH_2^- and NH^{2-} anions were not incorporated. These results clearly indicate that the incorporation of NH_2^- and NH^{2-} anions can be attributed to the presence of the unique nanoporous structure of mayenite crystals.

Figure 5a shows ^1H MAS NMR spectra of $Ca(NH_2)_2$ and CaNH crystals. $Ca(NH_2)_2$ exhibited two partially overlapping peaks between +0.0 and +3.0 ppm, both of which are attributed to the two hydrogen atoms in the amide group.[15] On the other hand, CaNH shows four or five broad peaks between −5 and +10 ppm. These broad bands were again due to the disordered H position in the CaNH crystal. Recently, Hayashi et al. reported that the chemical shift of ^1H nuclei is quite sensitive to

Table 1. Reaction Conditions and Properties of Parent and Ammonothermally Treated $C_{12}A_7{:}e^-$ and $C_{12}A_7{:}O^{2-}$

		ammonothermal condition			anion concentration (10^{20} cm^{-3})					
entry	parent	temp (°C)	pressure (MPa)	a (nm)	e^-	H^-	NH_2^-	NH^{2-}	OH^-	NH_x^{n-}/OH^- ratio[a]
1[b]	$C_{12}A_7{:}e^-_{half}$			1.1998	11.4					
2	$C_{12}A_7{:}e^-_{half}$	400	35	1.1995	11.0					
3	$C_{12}A_7{:}e^-_{half}$	500	45	1.1984	9.4	0.42	0.01	0.24	0.58	0.43
4	$C_{12}A_7{:}e^-_{half}$	600	55	1.1978	5.8	0.54	1.08	1.45	3.61	0.70
5[b]	$C_{12}A_7{:}e^-_{full}$			1.1999	22.5		0.00	0.00		
6	$C_{12}A_7{:}e^-_{full}$	600	55	1.1996	16.6	0.34	0.02	0.52	0.17	3.06
7[b]	$C_{12}A_7{:}O^{2-}$			1.1985	0.0		0.00	0.00		
8	$C_{12}A_7{:}O^{2-}$	600	55	1.1979	0.0	0.00	0.00	2.71	6.14	0.44

[a]Concentration ratio of encaged (NH_2^- + NH^{2-}) to encaged OH^-. [b]Samples before ammonothermal treatment.

dx.doi.org/10.1021/ja504185m | J. Am. Chem. Soc. 2014, 136, 11698–11706

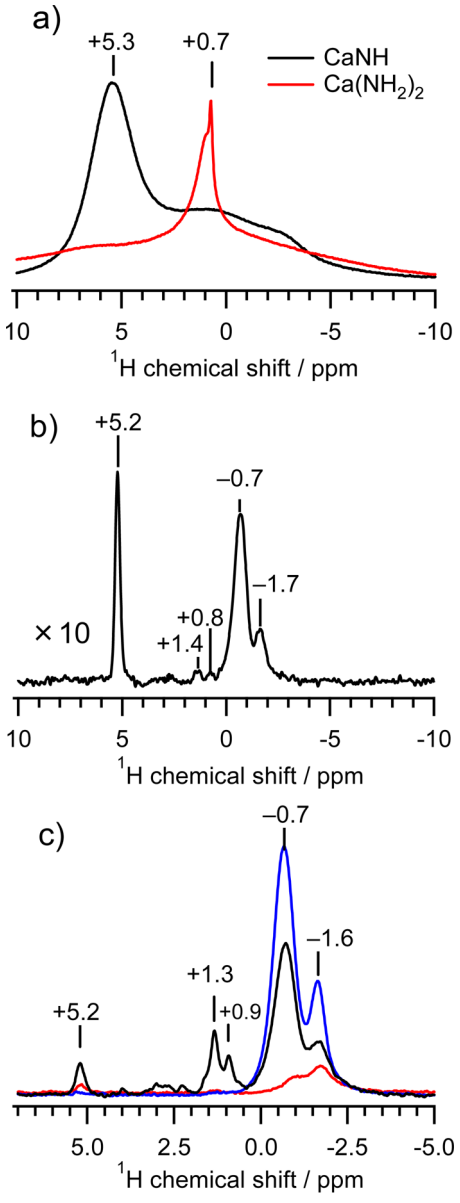

Figure 5. ^{1}H MAS NMR spectra of (a) CaNH and $Ca(NH_2)_2$ crystals, (b) $^{14}NH_3$-treated $C_{12}A_7{:}e^-_{half}$ at 500 °C, and (c) $^{14}NH_3$-treated $C_{12}A_7{:}e^-_{half}$ (black line), $C_{12}A_7{:}e^-_{full}$ (red line), and $C_{12}A_7{:}O^{2-}$ (blue line) at 600 °C.

the local environment in host compounds as well as the oxidation state, especially in the separation of interacting acceptor ions (i.e., O–H (or N–H)···acceptor separation).[25] When the charge state of H atom is positive (+1), the ^{1}H chemical shift is a function of O–H···acceptor separation. In contrast, when the charge state of H atom is negative (−1), the chemical shift is well-correlated with the H···acceptor separation. This point is clearly shown in Figure 4 of ref 25a. In the CaNH crystal shown in Figure S2b, Supporting Information, the H atoms of the imide groups are closely packed and disordered in the Ca octahedra, and this may be responsible for the peak broadness. Detail explanation will be presented in the later paragraph.

Figure 5b shows a ^{1}H MAS NMR spectrum of the $^{14}NH_3$-treated $C_{12}A_7{:}e^-_{half}$ at 500 °C (denoted $C_{12}A_7{:}NH^{2-}_{500°C,half}$), while Figure S4a, Supporting Information, shows the ^{1}H NMR spectrum of wet air-treated $C_{12}A_7{:}O^{2-}$ at 800 °C (denoted $C_{12}A_7{:}OH^-$), which was used as a reference. $C_{12}A_7{:}OH^-$ exhibited a sharp signal at −0.8 ppm, which can be assigned to the OH^- entrapped in the cage.[25] $C_{12}A_7{:}NH^{2-}_{500°C,half}$ gave three sharp signals at +5.2, −0.7, and −1.7 ppm. Figure 5c shows ^{1}H MAS NMR spectra of the $C_{12}A_7{:}e^-_{half}$, $C_{12}A_7{:}e^-_{full}$, and $C_{12}A_7{:}O^{2-}$ samples that were ammonothermally treated at 600 °C, and these were designated $C_{12}A_7{:}NH^{2-}_{600°C,half}$, $C_{12}A_7{:}NH^{2-}_{600°C,full}$, and $C_{12}A_7{:}NH^{2-}_{600°C,O^{2-}}$, respectively. Comparison of the result in Figure 5b with that in Figure 5c is shown in Figure S4b, Supporting Information. Figure S4b, Supporting Information, clearly indicated that the intensities of two signals at −0.7 and −1.6 ppm were significantly increased on the spectrum of $C_{12}A_7{:}NH^{2-}_{600°C,half}$. On the other hand, the intensity of signal at +5.2 ppm was not changed upon the 600 °C treatment. More importantly, the intensity order of the signal around −1.6 ppm is $C_{12}A_7{:}NH^{2-}_{600°C,O^{2-}}$ > $C_{12}A_7{:}NH^{2-}_{600°C,half}$ > $C_{12}A_7{:}NH^{2-}_{600°C,full}$ > $C_{12}A_7{:}NH^{2-}_{500°C,half}$ (Figure S4b$^-$), which is well correlated with the concentrations of nitrogen species determined by the IC and TPD analyses in Table 1. In contrast, the signal intensity at approximately +5.2 ppm was nearly the same among the four $C_{12}A_7{:}NH^{2-}$ samples, indicating that the signal at +5.2 ppm is not related to the nitrogen species.

The assignment of H species of ^{1}H NMR in solid is complex, that is, the chemical shift value is pretty sensitive to the local environment as well as the oxidation state. In our recent paper,[25] there is a clear correlation between the chemical shift and O–H (or N–H)···acceptor separation for proton. Namely, the chemical shift of H^+ decreases linearly with the separation distance because the electron density around the proton nuclei increases with increasing distance.[25] The NH^{2-} species in CaNH crystal is closely packed, wherein the NH···N separation is about 260 pm. On the other hand, the NH···O separation for the $C_{12}A_7{:}NH^{2-}$ is 290–310 pm (the separation value is dependent on the position of H atom in the cage), based on the assumption that the nitrogen atom is located in the center of the nanocage due to H atom rotation around N atom. It follows that the separation distance is longer in $C_{12}A_7{:}NH^{2-}$ than that in the CaNH crystal. This situation is very similar to that between $C_{12}A_7{:}OH^-$ and CaO-based compounds.[25] On the basis of these experimental results and theoretical consideration, we cannot assign the signal at +5.2 ppm to NH^{2-} dianion entrapped in the nanocage of mayenite, and instead we can safely assign the signal around −1.6 ppm to the NH^{2-} species for the $C_{12}A_7{:}NH^{2-}$ samples. On the other hand, the peak at +5.2 ppm observed for the $C_{12}A_7{:}NH^{2-}$ could be assigned to the H^- according to the report by Hayashi and coworkers: see Figure 4 in ref 25a. The two small peaks at +1.3 and +0.9 ppm could be attributed to the NH_2^- monoanion entrapped in the cage.

Figure 5c indicated that the intensity of NH^{2-} peak was dependent on the starting mayenite samples. This distinct difference in the intensities showed that the extraframework O^{2-} ion reacted more efficiently with NH_3 compared with the encaged electron. It is important to note here that the intensity ratio of the NH^{2-} peak around −1.6 ppm to OH^- at −0.7 ppm and the intensity of the H^- peak at +5.2 ppm also varied depending on the initial samples. This result suggests several reaction pathways in the ammonothermal reaction. Among the three samples, only $C_{12}A_7{:}NH^{2-}_{600°C,half}$ gave two signals at +0.9 and +1.3 ppm.

The reaction pathways that yield NH_2^- and NH^{2-} anions are next discussed so as to understand the dependence of NH^{2-}

dx.doi.org/10.1021/ja504185m | J. Am. Chem. Soc. 2014, 136, 11698–11706

concentration and anion distribution on the reactant samples. We considered two main reaction routes, that is, the reactions of NH_3 with the encaged O^{2-} ions or with the electrons. In the former, the pathways that yield NH_2^- and NH^{2-} are described by eqs 1 and 2.

$$NH_3 + O^{2-}{}_{cage} \rightarrow NH_2^-{}_{cage} + OH^-{}_{cage} \quad (1)$$

$$NH_2^-{}_{cage} + O^{2-}{}_{cage} \rightarrow NH^{2-}{}_{cage} + OH^-{}_{cage} \quad (2)$$

In these equations, the subscript "cage" indicates the species in the cage. In contrast, reactions involving the encaged electrons are described by eqs 3 and 4.

$$NH_3 + 2e^-{}_{cage} \rightarrow NH_2^-{}_{cage} + H^-{}_{cage} \quad (3)$$

$$NH_2^-{}_{cage} + 2e^-{}_{cage} \rightarrow NH^{2-}{}_{cage} + H^-{}_{cage} \quad (4)$$

According to the reactions shown in eqs 1 and 2, the concentration ratio of $NH_2^-{}_{cage}$ or $NH^{2-}{}_{cage}$ to $OH^-{}_{cage}$ should be 1:1 or 1:2, respectively. We calculated the concentration ratios of encaged NH_2^- and NH^{2-} to encaged OH^- (abbreviated NH_x^{n-}/OH^-), and the results are summarized in Table 1. The NH_x^{n-}/OH^- values for $C_{12}A_7{:}NH^{2-}{}_{500°C,half}$, $C_{12}A_7{:}NH^{2-}{}_{600°C,half}$, and $C_{12}A_7{:}NH^{2-}{}_{600°C,O^{2-}}$ were 0.43, 0.70, and 0.44, respectively (entries 3, 4, and 8 in Table 1). A good correlation with theoretical values (0.5−1.0) indicated that the main reaction pathways for $C_{12}A_7{:}O^{2-}$ and $C_{12}A_7{:}e^-{}_{half}$ are those in eqs 1 and 2. In contrast, the NH_x^{n-}/OH^- value for $C_{12}A_7{:}NH^{2-}{}_{600°C,full}$ was 3.06 (entry 6). The large NH_x^{n-}/OH^- value and the very low encaged OH^- concentration, which was ∼1/30th that of $C_{12}A_7{:}NH^{2-}{}_{600°C,O^{2-}}$, suggested that the main reaction pathways for $C_{12}A_7{:}e^-{}_{full}$ are those in eqs 3 and 4 instead of eqs 1 and 2. The enthalpy changes in reactions of eqs 1−4 are calculated and summarized in Table S2, entries 7−10, Supporting Information, on the basis of the reported data in the literature.[11d,25c] The enthalpy changes in the reactions for eqs 1−4 are −1.7, −0.8, −4.4, and −3.9 eV, respectively, and therefore the reactions in eqs 1−4 are thermodynamically feasible.

Encapsulated state of NH_2^- and NH^{2-}. It is well-accepted that in the absence of paramagnetic impurities ^1H spin relaxation is dominated by dipole−dipole coupling or a quadrupolar interaction.[26] This relaxation is accelerated by molecular motions like methyl group rotations leading to the reorientation of the dipolar vector.[27] ^1H T_1 is thus a benchmark to evaluate the dynamic motions of the hydrogen species. According to the theory of Bloembergen, Purcell, and Pound,[28] T_1 can be expressed by eq 5,

$$\frac{1}{T_1} = \left(\frac{2}{5}\right)\gamma^4 h^2 r^{-6} I(I+1)\left\{\frac{\tau}{(1+\omega^2\tau^2)} + \frac{4\tau}{(1+4\omega^2\tau^2)}\right\} \quad (5)$$

where γ is a gyromagnetic ratio, h is Planck's constant, r is the distance from the nucleus, I is the nuclear spin, ω is the Zeeman frequency, and t is the molecular motion correlation time. A short t, especially those close to Lamor's resonance frequency, allows for an energetic exchange between nuclear spins and the lattice, resulting in a decrease in T_1.

Figure S5a,b, Supporting Information, shows ^1H MAS NMR spectra of crystalline CaNH and $Ca(NH_2)_2$ as a function of the duration time τ. Figure S5c,d, Supporting Information, shows ^1H relaxation curves for the CaNH and $Ca(NH_2)_2$ wherein the analyzed signal positions are at +5.3 and +0.7 ppm, respectively. The plots in Figure S5c,d, Supporting Information, are inversely proportional to the relaxation rate $1/T_1$, indicating a single relaxation mechanism. The T_1 values that were determined by the inversion recovery method are summarized in Table 2. The T_1 values for CaNH and $Ca(NH_2)_2$ were 31.2 and 19.1 s, respectively. Figure S6a−d, Supporting Information, shows ^1H NMR spectra of $C_{12}A_7{:}NH^{2-}{}_{500°C,half}$, $C_{12}A_7{:}NH^{2-}{}_{600°C,half}$, $C_{12}A_7{:}NH^{2-}{}_{600°C,full}$, and $C_{12}A_7{:}NH^{2-}{}_{600°C,O^{2-}}$ samples as a function of τ, while Figure S7a−d, Supporting Information, shows ^1H relaxation curves for these $C_{12}A_7{:}NH^{2-}$ samples. The T_1 values of $C_{12}A_7{:}NH^{2-}$ are summarized in Table 2 as well. The ^1H T_1 of NH^{2-}, NH_2^-, OH^-, and H^- for the $C_{12}A_7{:}NH^{2-}$ samples were 8−19, 0.4, 22−28, and 42 s, respectively, and these are dependent on the host $C_{12}A_7{:}NH^{2-}$ samples. For example, the T_1 of NH^{2-} in $C_{12}A_7{:}NH^{2-}{}_{600°C,half}$ was ∼8 s, while that in $C_{12}A_7{:}NH^{2-}{}_{600°C,O^{2-}}$ was ∼19 s. Although the details are not yet completely understood, this variation can be attributed to differences in the local environment of the lattice cage that accommodates the encaged NH^{2-}, which can permit an energy exchange upon relaxation. The order of T_1 was here $NH_2^- < NH^{2-} < OH^- < H^-$ in the cages.

Table 2. ^1H Spin−Lattice Relaxation Times for Various Anions Embedded in the Crystalline CaNH, $Ca(NH_2)_2$, and $C_{12}A_7{:}NH^{2-}$ Samples

sample	embedded anion	T_1, s^{-1}
CaNH	NH^{2-}	31.2
$Ca(NH_2)_2$	NH_2^-	19.1
$C_{12}A_7{:}NH^{2-}{}_{500°C,half}$	NH^{2-}	18.3
	OH^-	24.7
	H^-	41.9
$C_{12}A_7{:}NH^{2-}{}_{600°C,half}$	NH^{2-}	0.4
	NH_2^-	8.4
	OH^-	28.3
$C_{12}A_7{:}NH^{2-}{}_{600°C,full}$	NH^{2-}	14.3
$C_{12}A_7{:}NH^{2-}{}_{600°C,O^{2-}}$	NH^{2-}	18.9
	OH^-	22.2

Another important point in Table 2 is that the encapsulation of anions in the nanocages led to a short T_1 for the amide and the imide ions. For instance, the T_1 values for NH_2^- (0.4 s) and NH^{2-} (8−19 s) in $C_{12}A_7{:}NH^{2-}$ were significantly shorter than those for crystalline $Ca(NH_2)_2$ (19 s) and CaNH (32 s). Matsuishi et al. reported that encaged superoxide ions O_2^- with size of ∼0.26 nm in diameter make a precessional motion in the mayenite crystal nanocage around ambient temperatures.[29] Taking into account the similar anion sizes of O_2^-, NH_2^-, and NH^{2-} (see Table S1, Supporting Information), both NH_2^- and NH^{2-} with an ∼0.26 nm diameter could dynamically rotate in the cage. A similar encapsulation effect leading to a shorter T_1 was reported for CO_3^{2-} in the interlayer of a layered double hydroxide (LDH).[30] The intercalated CO_3^{2-} in LDH gave a ^{13}C T_1 relaxation time of ∼160 s, which is 12.5 times shorter than that for ^{13}C-labeled sodium carbonate crystals (∼2000 s). Therefore, the shorter ^1H T_1 of NH_2^- and NH^{2-} in $C_{12}A_7{:}NH^{2-}$ that comes from encapsulation may be attributed to the dynamic motions of nitrogen species in the nanocage.

Figure 6 and Figure S8, Supporting Information, show ^{15}N CP- and DD-MAS NMR spectra of $C_{12}A_7{:}NH^{2-}{}_{600°C,O^{2-}}$. A single signal was present at −324 ppm because of NH^{2-} in both

dx.doi.org/10.1021/ja504185m | J. Am. Chem. Soc. 2014, 136, 11698−11706

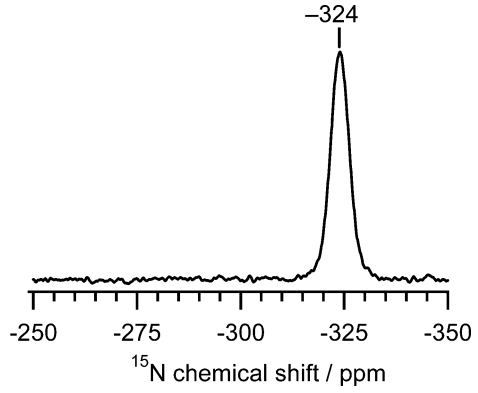

Figure 6. ^{15}N CP-MAS NMR spectrum of $^{15}NH_3$-treated $C_{12}A_7{:}O^{2-}$ at 600 °C.

these figures. The position of the encaged $\underline{N}H^{2-}$ is very close to that (−329 ppm with reference to $^{15}NH_4Cl$)[31] of Mg$\underline{N}$H.[2] More importantly, the full width at half-maximum (fwhm) for this signal was only ∼5 ppm (Figure 6), which is about 1/5th that of MgNH.[2] This narrow fwhm can also be attributed to the rotating nitrogen species in the nanocage.

Chemical Stability and Potential Applications. The chemical stability of the encaged NH^{2-} diainon was studied under different treatment conditions. Figure 7 shows Raman

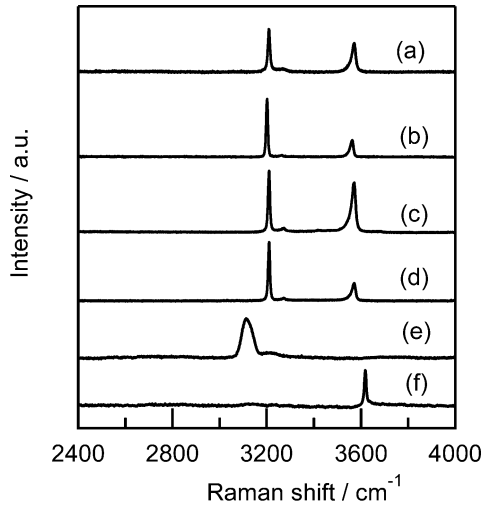

Figure 7. Raman spectra of fresh $C_{12}A_7{:}NH^{2-}{}_{600°C,O^{2-}}$ (a), $C_{12}A_7{:}NH^{2-}{}_{600°C,O^{2-}}$ stored in air for 40 days (b), $C_{12}A_7{:}NH^{2-}{}_{600°C,O^{2-}}$ immersed in MeOH (c) or THF (d), fresh CaNH (e), and CaNH stored in air for 10 min (f). The NH^{2-} concentrations of the stored and solvent-treated $C_{12}A_7{:}NH^{2-}$ (∼2.60 × 10^{20} cm^{-3}) were comparable to that of the fresh $C_{12}A_7{:}NH^{2-}{}_{600°C,O^{2-}}$.

spectra of $C_{12}A_7{:}NH^{2-}$ after treatments along with those for the CaNH crystal. Even after treatments, all the $C_{12}A_7{:}NH^{2-}$ samples had a sharp signal at 3210 cm^{-1}, and this is assignable to the NH^{2-} ion in which the nitrogen concentrations of $C_{12}A_7{:}NH^{2-}$ were similar after the treatment. In contrast, even after 10 min storage under ambient conditions, the NH band around 3140 cm^{-1} for CaNH disappeared and instead the band at 3610 cm^{-1}, which is assignable to OH stretching, was enhanced, indicating extreme low chemical instability. This notable difference indicates the superior chemical stability of $C_{12}A_7{:}NH^{2-}$ against oxygen and organic solvents, which comes from the encapsulation of NH^{2-} in the crystallographic cages of mayenite.

Figure 8a shows the TPD profile (m/z = 16) of $^{14}NH_3$-treated $C_{12}A_7{:}O^{2-}$ (entry 8 in Table 1). Note that the mass

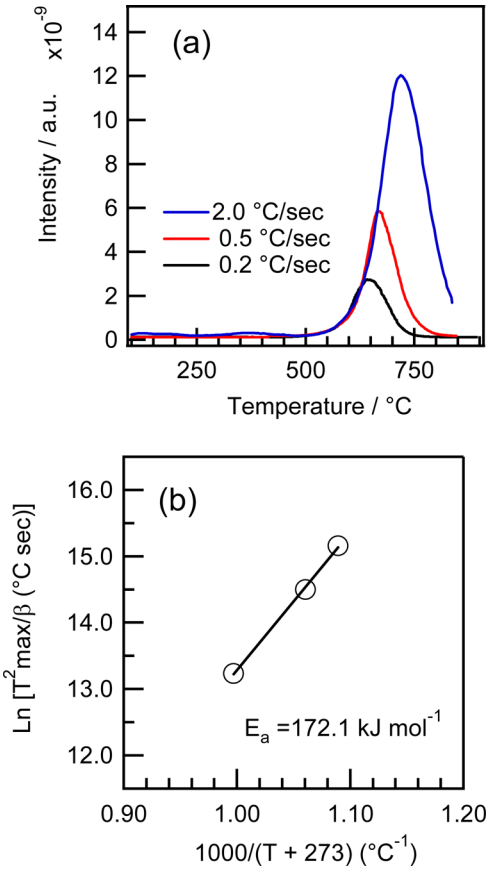

Figure 8. (a) Thermal desorption profile of NH_3 (m/z = 16) from the $^{14}NH_3$-treated $C_{12}A_7{:}O^{2-}$ at 600 °C (entry 8 in Table 1). Heating rates were 0.2, 0.5, and 2.0 °C s^{-1}. (b) Activation energy, E_a, estimation of NH_3 desorption from $C_{12}A_7{:}NH^{2-}{}_{600°C,O^{2-}}$ using the Redhead equation. T_{max} = temperature corresponding to the peak of the NH_3 desorption band, which was the maximum NH_3 desorption. E_a was estimated to be 172 kJ mol^{-1}.

fragmentation pattern of the desorbed species is almost the same as that for an NH_3 molecule, indicating that the desorbed species is NH_3 and not NH^{2-}, presumably through the reverse reactions shown in eqs 1 and 2. The TPD profile yielded a symmetrical peak indicative of a pseudo-second-order reaction in which NH_3 desorption started at around 500 °C. To estimate the activation energy (E_a) for NH_3 desorption, a plot of $\ln(T_{max}{}^2/\beta)$ versus $1/T_{max}$ (T_{max} = temperature of signal maximum, β = heating rate) was compiled for $C_{12}A_7{:}NH^{2-}{}_{600°C,O^{2-}}$ as shown in Figure 8b. This followed the Redhead model for second-order desorption.[32] The estimated E_a was 172 kJ mol^{-1}, which is about twice as large as that (76−100 kJ mol^{-1}) for the surface of TiO_2(110) plane and of aluminum silicates.[33] The on-set temperature of NH_3 desorption from $C_{12}A_7{:}NH^{2-}$ was 250−350 °C higher than that for aluminum silicates and Ca−Mg−N−H compounds.[33,34] The higher E_a and higher desorption temperatures are due to the effect of NH^{2-} encapsulation by the rigid Ca−O−Al oxide frameworks. The TG-DTA profile of $C_{12}A_7{:}NH^{2-}{}_{600°C,O^{2-}}$ is shown in Figure S9, Supporting

dx.doi.org/10.1021/ja504185m | J. Am. Chem. Soc. 2014, 136, 11698−11706

Information. The weight loss was ∼0.1 wt % between 50 and 700 °C, indicating that the entrapped NH^{2-} was not completely desorbed at ambient pressure conditions. Besides, at or above 750 °C, the weight of $C_{12}A_7$:NH^{2-} was increased primarily due to the reaction with trace amounts of H_2O as shown in eq 6.

$$NH^{2-}{}_{cage} + H_2O \rightarrow NH_2^-{}_{cage} + OH^-{}_{cage} \quad (6)$$

Note that the TPD analysis was carried at $\sim 10^{-6}$ Pa. This difference in the NH_3 desorption could be attributed to the high activation energy of NH_3 desorption from the nanocage of mayenite crystals.

Finally, we discuss the outlook for the application of $C_{12}A_7$:NH^{2-} samples to chemical reactions. The introduction of nitrogen functional groups is quite important for the production of pharmaceutical and agricultural products. In particular, reductive (hydro)amination and amidation using a simple N1 source like NH_3 are challenging subjects in organic synthetic chemistry.[35] Our group reported that two kinds of electride, $C_{12}A_7$:e^- and Ca_2N:e^-, act as an efficient electron donor, which can promote the pinacol coupling of aldehydes in aqueous or alcoholic solvents.[36,37] In these reactions, polar substrates like aldehydes are selectively adsorbed onto the surface of the electride, and the addition of water or methanol leads to cage or 2D layer rupture and subsequent in situ electron formation. This allows selective electron transfer from the electride to the carbonyl carbon atoms of the aldehyde resulting in the acceleration of coupling reactions. Similarly, encaged NH^{2-} in $C_{12}A_7$:NH^{2-} might selectively react with polar carbon groups of substrates on site under controlled reaction conditions. This reaction can lead to nitrogen transfer reactions, including the synthesis of primary amines and amides. It is thus expected that $C_{12}A_7$:NH^{2-} functions as a single N1 source reagent like Grignard reagents. Relevant studies are now in progress.

CONCLUSIONS

We succeeded in encapsulating reactive NH^{2-} dianions within the subnanocages of mayenite crystals by ammonothermal treatment. The incorporated NH^{2-} content and concentration were ∼0.25 $(\text{wt \%})_{NH}$ (∼0.2 mmol g^{-1}) and $\sim 2.7 \times 10^{20}$ cm^{-3}, respectively. Raman spectroscopic analysis indicated that the bond strength of the encaged NH^{2-} in $C_{12}A_7$:NH^{2-} is comparable to that of NH^{2-} in MgNH and CaNH crystals. ^1H MAS NMR spectroscopic analyses showed several reaction pathways leading to NH^{2-} and NH_2^-. The short spin−lattice relaxation time of $C_{12}A_7$:NH^{2-} indicated the dynamic rotation of NH^{2-} and NH_2^- entrapped in the mayenite crystal cages, as was found for encaged O_2^-. A chemical stability test revealed the remarkable stability of $C_{12}A_7$:NH^{2-} toward oxygen and organic solvents, and this is attributed to encapsulation by a robust nanocage composed of Ca−O−Al oxide. Raman experiments as well as ^1H and ^{15}N NMR results suggest the potential application of $C_{12}A_7$:NH^{2-} to a single N1 source reagent for amination and amidation reactions.

ASSOCIATED CONTENT

Supporting Information

Size of anions, XRD patterns, structural data, $M-T$ curves, ^1H MAS and ^{15}N-DD-MAS NMR spectra, and TG-DTA profile. This material is available free of charge via the Internet at http://pubs.acs.org.

AUTHOR INFORMATION

Corresponding Authors

fhayash@lucid.msl.titech.ac.jp
hosono@msl.titech.ac.jp

Present Address

[⊥]F.H.: Center for Energy and Environmental Science, Shinshu University, Nagano, Japan.

Notes

The authors declare no competing financial interest.

ACKNOWLEDGMENTS

This work was supported by the JST Accel Program and the JSPS Funding Program for World-Leading Innovative R&D on Science and Technology (FIRST), Japan. We are grateful to Drs. Satoru Matsuishi and Katsuro Hayashi (Tokyo Institute of Technology) for their helpful discussions.

REFERENCES

(1) (a) Chen, P.; Xiong, Z.; Luo, J.; Lin, J.; Tan, K. L. *Nature* **2002**, *420*, 302. (b) Gregory, D. H. *J. Mater. Chem.* **2008**, *18*, 2321.

(2) Ash-Kurlander, U. G.; Shter, E.; Kababya, S.; Schmidt, A.; Grader, G. S. *J. Phys. Chem. C* **2013**, *117*, 1237.

(3) Baba, T.; Kim, G. J.; Ono, Y. *J. Chem. Soc., Faraday Trans.* **1992**, *88*, 891.

(4) Okachi, T.; Onaka, M. *J. Am. Chem. Soc.* **2004**, *126*, 2306.

(5) Mal, P.; Breiner, B.; Rissanen, K.; Nitschke, J. R. *Science* **2009**, *324*, 1697.

(6) For representative reviews on the anion receptors, see: (a) Wenzel, M.; Hiscock, J. R.; Gale, P. A. *Chem. Soc. Rev.* **2012**, *41*, 480. (b) Ballester, P. *Chem. Soc. Rev.* **2010**, *39*, 3810. (c) Amouri, H.; Desmarets, C.; Moussa, J. *Chem. Rev.* **2012**, *112*, 2015.

(7) Hosono, H.; Abe, Y. *Inorg. Chem.* **1987**, *26*, 1192.

(8) (a) Hayashi, K.; Matsuishi, S.; Kamiya, T.; Hirano, M.; Hosono, H. *Nature* **2002**, *419*, 462. (b) Williams, P. P. *Acta Crystallogr.* **1973**, *B29*, 1550. (c) Miyakawa, M.; Kamioka, H.; Hirano, M.; Kamiya, T.; Sushko, P. V.; Shluger, A. L.; Matsunami, N.; Hosono, H. *Phys. Rev. B* **2006**, *73*, No. 205108.

(9) Matsuishi, S.; Toda, Y.; Miyakawa, M.; Hayashi, K.; Kamiya, T.; Hirano, M.; Tanaka, I.; Hosono, H. *Science* **2003**, *301*, 626.

(10) Dye, J. L. *Acc. Chem. Res.* **2009**, *42*, 1564.

(11) (a) Boysen, H.; Kaiser-Bischoff, I.; Lerch, M. *Diffus. Fundam* **2008**, *8*, 2.1. (b) Boysen, H.; Kaiser-Bischoff, I.; Lerch, M.; Berendts, S.; Börger, A.; Trots, D. M.; Hoelzel, M.; Senyshyn, A. *Z. Kristallogr. Suppl.* **2009**, *30*, 323. (c) Boysen, H.; Kaiser-Bischoff, I.; Lerch, M.; Berendts, S.; Hoelzel, M.; Senyshyn, A. *Acta Phys. Polym., A* **2010**, *117*, 38. (d) Polfus, J. M.; Toyoura, K.; Hervoches, C. H.; Sunding, M. F.; Tanaka, I.; Haugsrud, R. *J. Mater. Chem.* **2012**, *22*, 15828.

(12) Peer, W. J.; Lagowski, J. J. *J. Phys. Chem.* **1980**, *84*, 1110.

(13) Lagowski, J. J. *Synth. React. Inorg., Met.-Org., Nano-Met. Chem.* **2007**, *37*, 115.

(14) Kim, S. W.; Matsuishi, S.; Nomura, T.; Kubota, Y.; Takata, M.; Hayashi, K.; Kamiya, T.; Hirano, M.; Hosono, H. *Nano Lett.* **2007**, *7*, 1138.

(15) Senker, J.; Jacobs, H.; Müller, M.; Press, W.; Mayer, H. M.; Ibberson, R. M. *Z. Anorg. Allg. Chem.* **1999**, *625*, 2025.

(16) Sichla, T.; Jacobs, H. *Z. Anorg. Allg. Chem.* **1996**, *622*, 2079.

(17) Yoshizumi, T.; Matsuishi, S.; Kim, S. W.; Hosono, H.; Hayashi, K. *J. Phys. Chem. C* **2010**, *114*, 1534.

(18) Hayashi, F.; Ishizu, K.; Iwamoto, M. *J. Am. Ceram. Soc.* **2010**, *93*, 104.

(19) Hayashi, F.; Toda, Y.; Kanie, Y.; Kitano, M.; Inoue, Y.; Yokoyama, T.; Hara, M.; Hosono, H. *Chem. Sci.* **2013**, *4*, 3124.

(20) Hayashi, K.; Hirano, M.; Hosono, H. *J. Phys. Chem. B* **2005**, *109*, 11900.

(21) Senker, J.; Jacobs, H.; Müller, M.; Press, W.; Müller, P.; Mayer, H. M.; Ibberson, R. M. *J. Phys. Chem. B* **1998**, *102*, 931.

(22) Kojima, Y.; Kawai, Y. *Chem. Commun.* **2004**, *40*, 2210.
(23) (a) Linde, G.; Juza, R. *Z. Anorg. Allg. Chem.* **1974**, *409*, 199. (b) Liu, Y.; Liu, T.; Xiong, Z.; Hu, J.; Wu, G.; Chen, P.; Wee, A. T. S.; Yang, P.; Murata, K.; Sakata, K. *Eur. J. Inorg. Chem.* **2006**, *2006*, 4368.
(24) Nomura, T.; Hayashi, K.; Kubota, Y.; Kamiya, T.; Hirano, M.; Takata, M.; Hosono, H. *Chem. Lett.* **2007**, *36*, 902.
(25) (a) Hayashi, K.; Sushko, P. V.; Hashimoto, Y.; Shluger, A. L.; Hosono, H. *Nat. Commun.* **2014**, *5*, 3515. (b) Hayashi, K. *J. Solid State Chem.* **2011**, *184*, 1428. (c) Hayashi, K.; Hirano, M.; Hosono, H. *Bull. Chem. Soc. Jpn.* **2007**, *80*, 872.
(26) Bakhmutov, V. I. *Solid-State NMR in Materials Science: Principles and Applications*; CRC Press: Boca Raton, FL, 2012; pp 149−164.
(27) Müller-Warmuth, W.; Schüler, R. *J. Magn. Reson.* **1979**, *34*, 83.
(28) Bloembergen, N.; Purcell, E. M.; Pound, R. V. *Phys. Rev.* **1948**, *73*, 679.
(29) Matsuishi, S.; Hayashi, K.; Hirano, M.; Tanaka, I.; Hosono, H. *J. Phys. Chem. B* **2004**, *108*, 18557.
(30) Ishihara, S.; Sahoo, P.; Deguchi, K.; Ohki, S.; Tansho, M.; Shimizu, T.; Labuta, J.; Hill, J. P.; Ariga, K.; Watanabe, K.; Yamauchi, Y.; Suehara, S.; Iyi, N. *J. Am. Chem. Soc.* **2013**, *135*, 18040.
(31) Hayashi, S.; Hayamizu, K. *Bull. Chem. Soc. Jpn.* **1991**, *64*, 688.
(32) (a) Redhead, P. A. *Vacuum* **1962**, *12*, 203. (b) Amenomiya, Y. R.; Cvetanovic, J. *J. Phys. Chem.* **1963**, *67*, 144.
(33) (a) Farfan-Arribas, E.; Madix, R. J. *J. Phys. Chem. B* **2003**, *107*, 3225. (b) Arenaa, F.; Dario, R.; Parmaliana, A. *Appl. Catal., A* **1998**, *170*, 127.
(34) Liu, Y.; Hu, J.; Xiong, Z.; Wu, G.; Chen, P.; Murata, K.; Sakata, K. *J. Alloy. Compd.* **2007**, *432*, 298.
(35) For representative reviews on the nitrogen transfer reactions, see (a) Klinkenberg, J. L.; Hartwig, J. F. *Angew. Chem., Int. Ed.* **2011**, *50*, 86. (b) Vlugt, J. I. *Chem. Soc. Rev.* **2010**, *39*, 2302.
(36) Buchammagari, H.; Toda, Y.; Hirano, M.; Hosono, H.; Takeuchi, D.; Osakada, K. *Org. Lett.* **2007**, *9*, 4287.
(37) Kim, Y. J.; Kim, S. M.; Hosono, H.; Yang, J. W.; Kim, S. W. *Chem. Commun.* **2014**, *50*, 4791.